Supplementary Information (SI) of

Downwind evolution of the volatility and mixing state of near-road aerosols near a US interstate highway

Provat Kumar Saha[1], Andrey Khlystov[2], and Andrew Patrick Grieshop[1]

[1]Department of Civil, Construction and Environmental Engineering, North Carolina State University, Raleigh, North Carolina, USA

[2]Division of Atmospheric Sciences, Desert Research Institute, Reno, Nevada, USA

Correspondence to: A. P. Grieshop (apgriesh@ncsu.edu)

S1: Supplementary figures

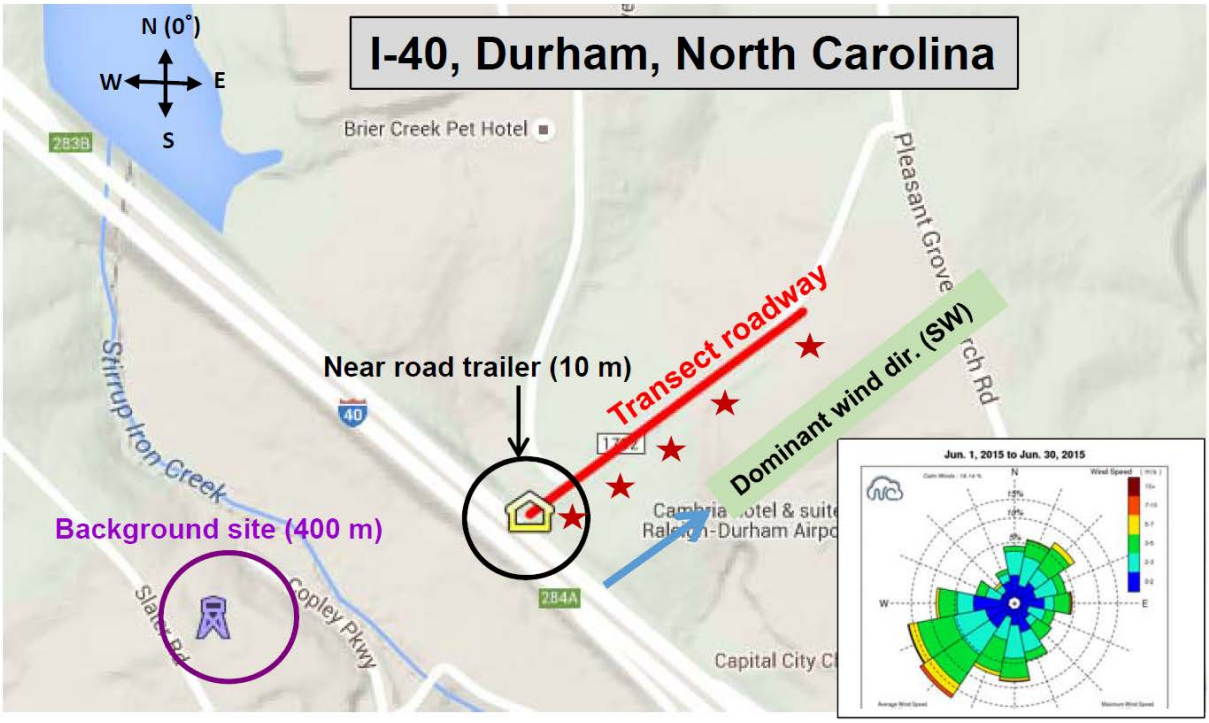

Figure S1: Study area map showing near-road trailer, transect roadway and upwind background site. Wind rose plot (inset) is shown for the I-40 summer campaign period (June 1 to June 30, 2015). Image: Google Maps

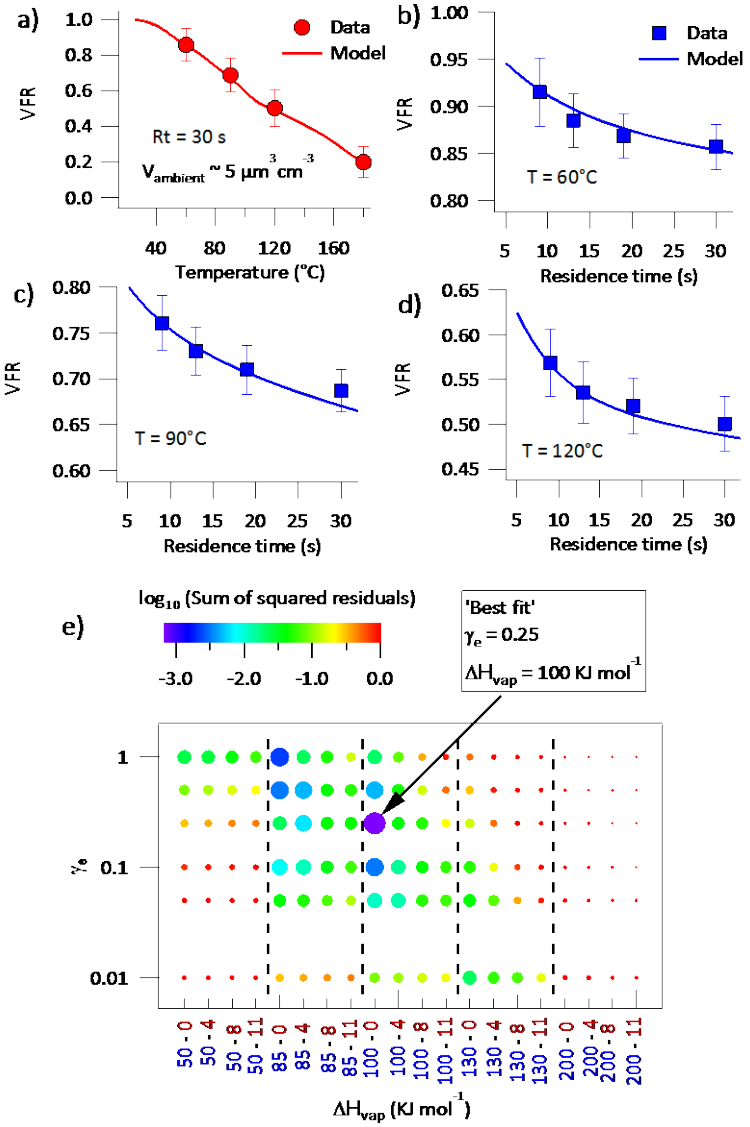

Figure S2: (a-d) Measured (point) and modeled (line) campaign-average VFR of $PM_{0.4}$ (integrated volume; 10-400 nm) as a function of TD temperatures and residence times. Measurements were collected in summer 2015 at 10 m distance from the highway. The point is mean, and error bar is ± one standard deviation (~15 minute time resolution data) at each temperature and Rt condition. (e) The goodness of fit (sum of squared residuals; SSR) associated with evaporation kinetics model fits to campaign average observations over a wide ranging (ΔH_{vap} γ_e) space. A larger marker size indicates a better fit. The x-axis of panel (e) represents ΔH_{vap} as, ΔH_{vap} = intercept-slope ($\log_{10}C^*$) (e.g., 50-0 on x-axis indicates intercept = 50 and slope = 0). Fitting approach is described in detail in Saha et al. (2015). Model lines in panels (a-d) are shown using the 'best fit' parameter values (ΔH_{vap} = 100 kj mol^{-1}, γ_e = 0.25, and corresponding fitted volatility distribution).

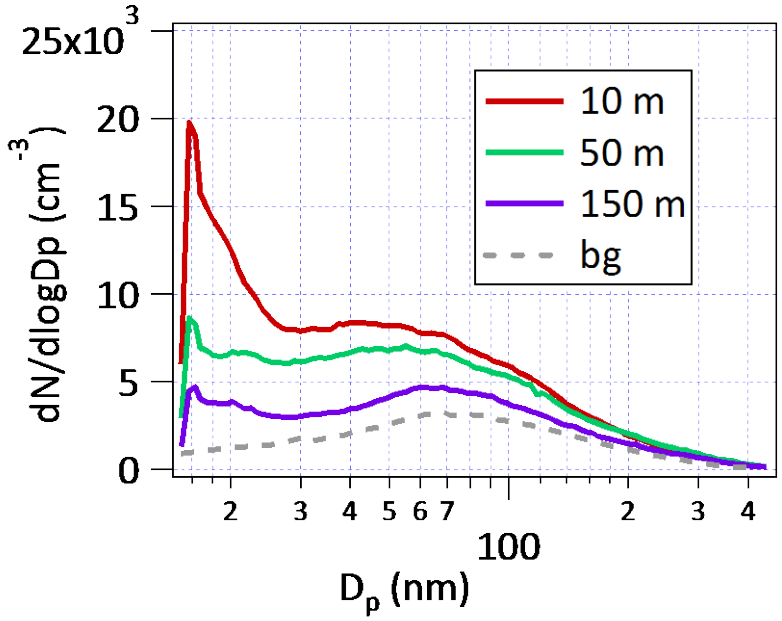

Figure S3: Particle number size distributions at different distances from highway I-40. Example measurements are shown from the I-40 summer campaign. The background (bg) measurement was collected at approximately 400 m 'upwind' from the main roadside monitor station on the opposite side of I-40.

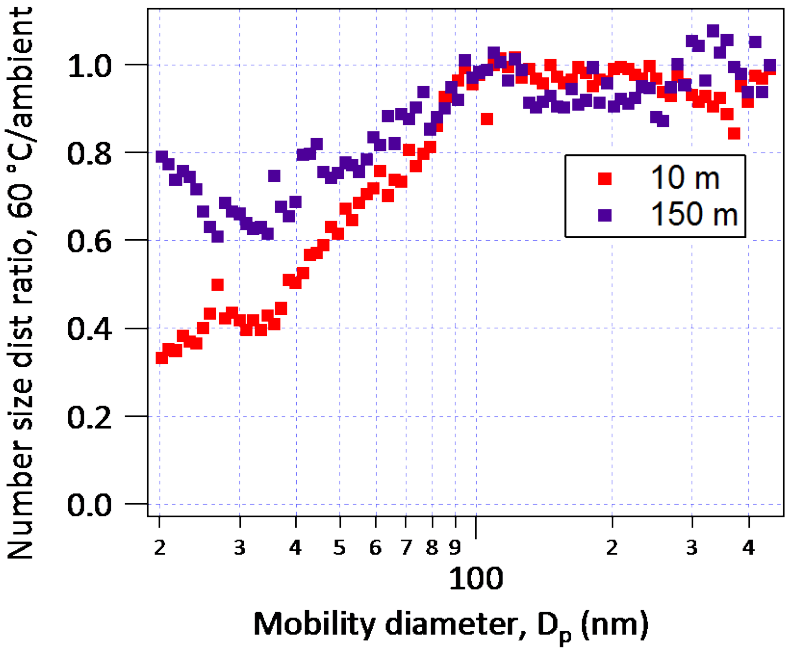

Figure S4: Ratio of particle number size distributions (dN/dlogDp) after heating at 60ºC in a thermodenuder (TD) to that at ambient temperature. Example measurements are shown from the I-40 summer campaign. Before ratio estimation, particle loss correction factors (as a function of size) were applied to the TD data.

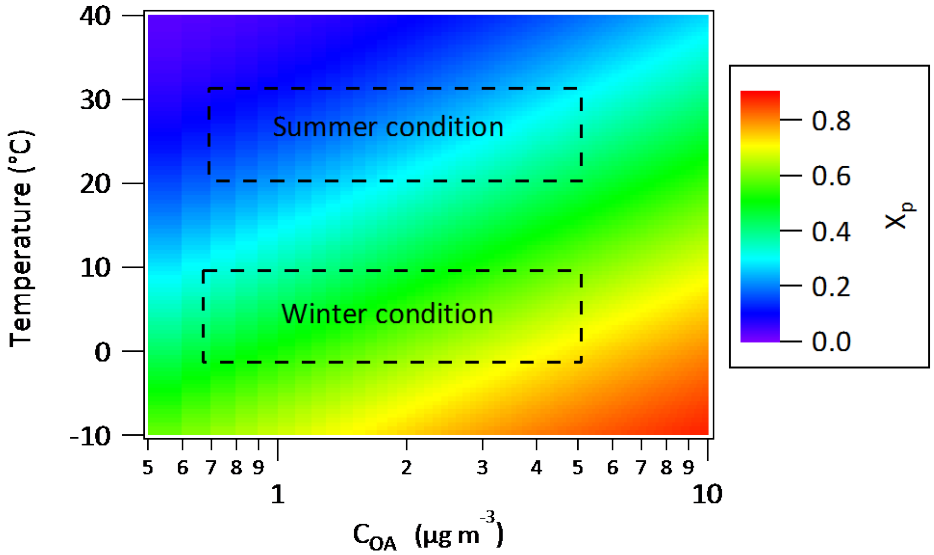

Figure S5: Temperature sensitivity of gas-particle partitioning of semi-volatile emissions from motor vehicles. Partitioning calculation uses gasoline POA volatility distribution from May et al. (2013) (TD-GC-MS derived median distribution) and ΔHvap from Ranjan et al. (2012) and method as described in May et al.(2013) and Donahue et al. (2006). X_p refer the fraction of semi-volatile organic mass in the particle-phase.

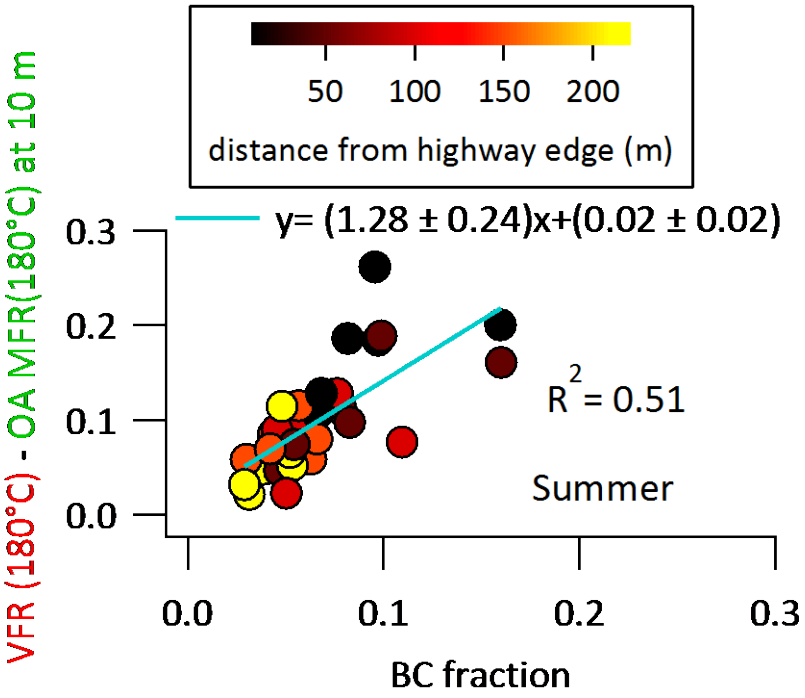

Figure S6: Similar to Figure 2(c) in main text, showing analysis for the summer data set. Correlation between the downwind evolution of BC fraction and VFR of $PM_{0.4}$ (at 180 ºC) after subtracting OA MFR (at 180ºC) measured at 10 m using TD/ACSM.

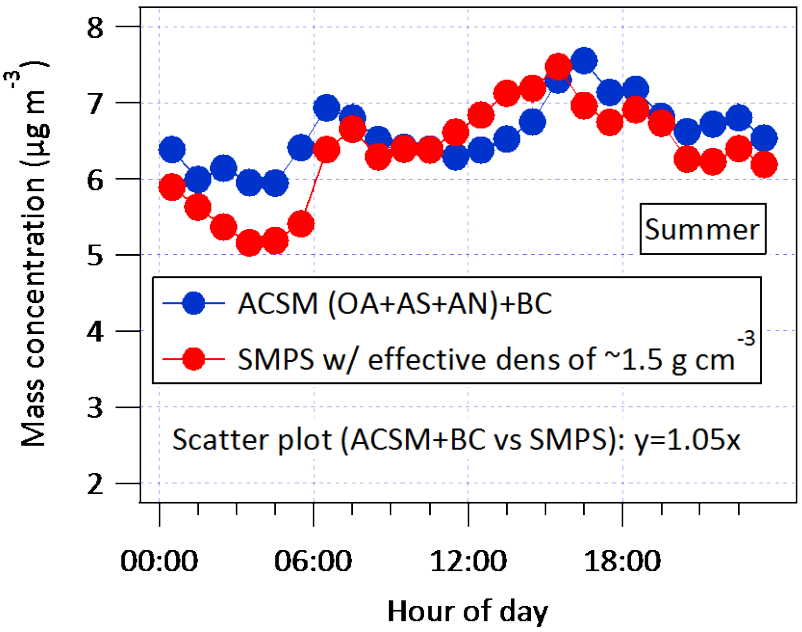

Figure S7: Comparison of diurnal average submicron ambient aerosol mass concentrations measured by SMPS with the concentrations measured by ACSM [organic aerosol (OA) + ammonium sulfate (AS) + ammonium nitrate (AN)] + PAX [black carbon (BC)]. Campaign-average diurnal profile is shown from summer campaign. ACSM data were analyzed using a collection efficiency (CE) of 1 for all species. AS mass concentration (m_{as}) is calculated as $\frac{132}{96} \times m_{SO4}$, where m_{SO4} is the mass concentration of sulfate (SO_4). AN mass concentration (m_{an}) is calculated as $\frac{80}{62} \times m_{NO3}$, where m_{NO3} is the mass concentration of nitrate (SO_4). SMPS mass concentrations were based on an estimated effective density of submicron aerosols of 1.5 cm^{-3}. The effective density is calculated by weighting fractional contribution of different species (e.g., campaign average: OA ~74%, AS ~13%, AN ~7%, and BC ~6%) with their respective densities. An effective density of OA of 1.45 g cm^{-3}, estimated from a parameterization using elemental composition (O:C; H:C) (Kuwata et al., 2012). Assumed densities for AS, AN, and BC were 1.77, 1.72 and 1.8 g cm^{-3}, respectively.

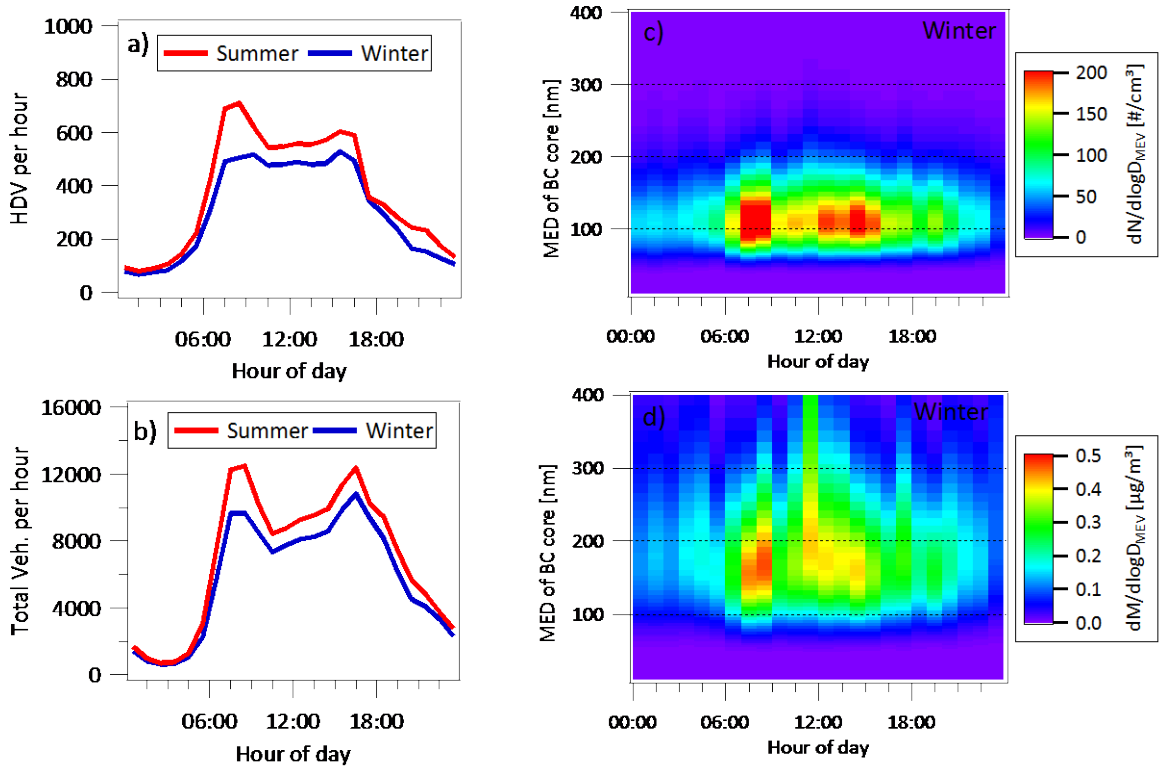

Figure S8: (a-b) Campaign-average diurnal profile of traffic volume: a) heavy duty vehicle (HDV), b) total vehicle. (c-d) Campaign-average diurnal profile of SP2-measured BC size distribution: c) number-weighted distribution, d) mass-weighted distribution; MED is the mass equivalent diameter. SP2 data were collected at the roadside trailer (10 m from highway edge) during the I-40 winter campaign only.

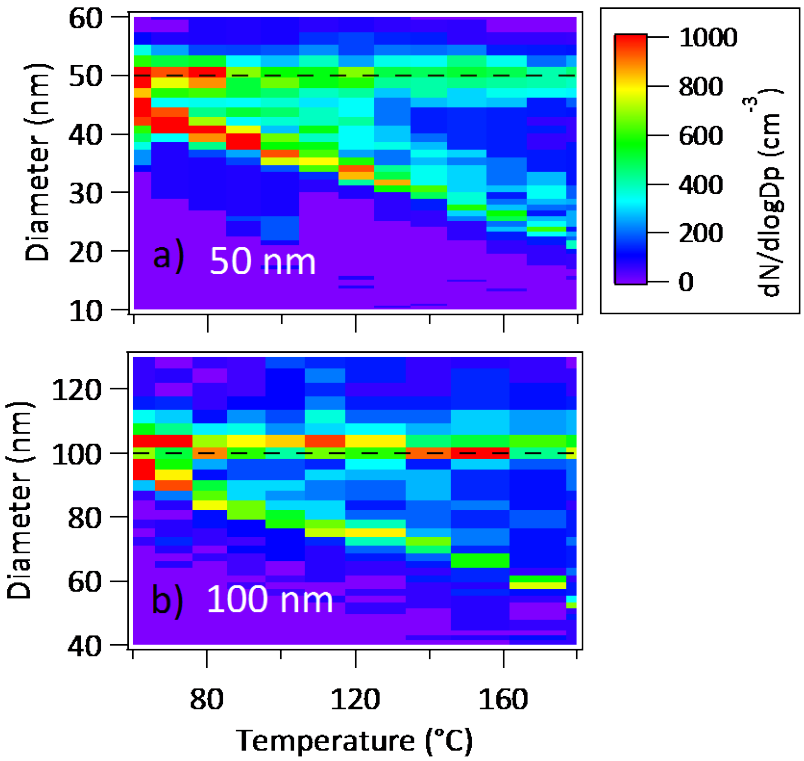

Figure S9: Similar to Figure 3 in main text, showing average volatility spectra of 50, and 100 nm particles collected at 10 m distance during the I-40 winter campaign.

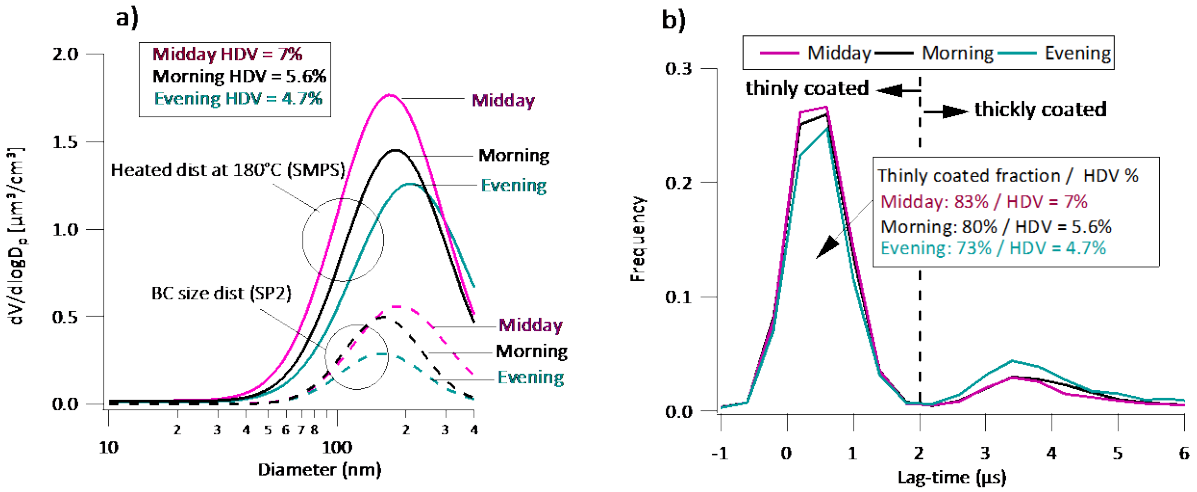

Figure S10: (a) Temporal variation of SP2-measured BC size distribution and volume-weighted SMPS size distribution after heating at 180 ºC in a thermodenuder. (b) Temporal variation of the frequency distributions (histograms) of SP2 lag-time ($\Delta\tau$). The analysis shown here is based on an example data set collected at 10 m downwind distance on February 10, 2016 with the wind consistently coming off of the highway.

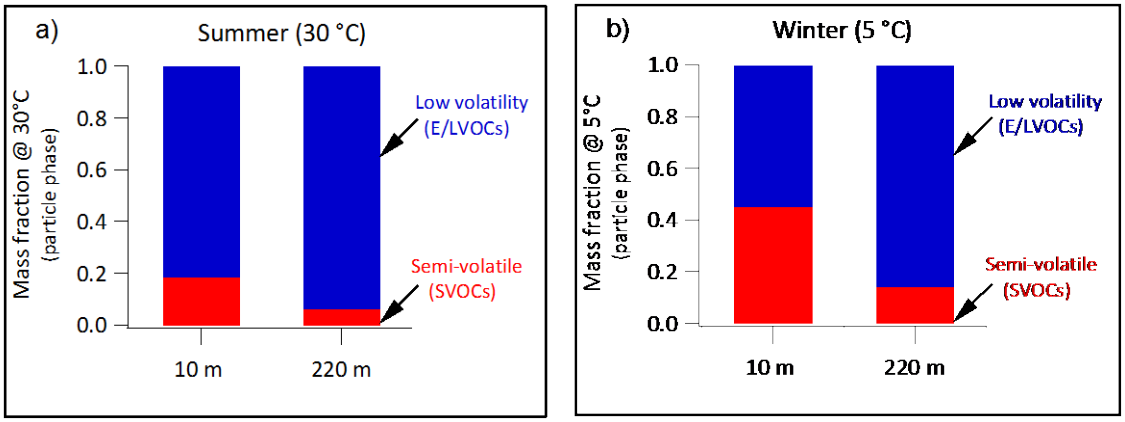

Figure S11: Similar to Figure 7 in the main text, showing volatility classification of near-road particles measured at 10 m and 220 m at campaign-average ambient temperature of ~5 ºC in winter and ~30ºC in summer. Distributions of particle-phase material are shown using two broad volatility categories. Partitioning calculation used a ΔH_{vap} of 100 kj mol^{-1}, Clausius–Clapyeron equation and equlibrium partitioning theory (Donahue et al., 2006) for estimating volatility distributions at campaign-average ambient temperatures.

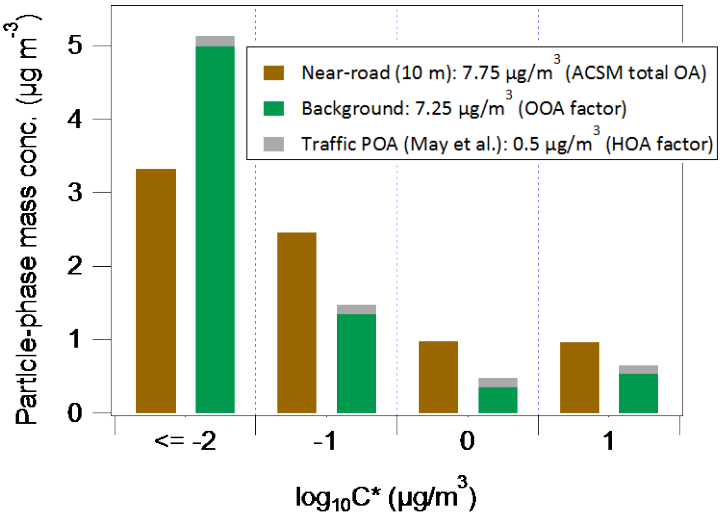

Figure S12: Similar to Figure 8b in the main text. In this analysis, traffic and background OA are apportioned from tracer m/z based factor analysis (Ng et al., 2011) of ACSM-measured mass spectra data at the roadside location. Hydrocarbon-like OA (HOA) is considered as traffic OA and oxygenated-OA (OOA) is considered as background OA. To be consistent with Figure 8, this analysis also considered data from the morning period on June 12, 2015. Figure shows distributions of OA mass loading (particle-phase only) as measured at 10 m downwind using ACSM (brown bar) and apportioned to vehicle emissions (grey) and background (green) volatility distributions using distributions from May et al. (2013a) and fits to downwind (220 m) TD data, respectively.

S2: Supplementary tables

Table S1: Assumed TD kinetic model input parameters*

Parameters	Value
Density (kg m^{-3})	1100
Diffusion coefficient (m^2 s^{-1})	5 E-06
Surface tension (J m^{-2})	0.05
Molecular weight (MW) g mol^{-1}	200

*assumed values similar as used in May et al. (2013) for TD modelling

Table S2: TD-derived volatility distribution (at 25ºC) of near-road aerosols (particle-phase distribution) at 10 m and 220 m downwind distance from the highway I-40 during summer and winter

logC* at 298K	[a]Particle-phase distribution (x_i)			
	Derived from fitting of observed evaporation of size-selected particles			
	10 m (summer)	220 m (summer)	10 m (winter)	220 m (winter)
	Combined (25,50,100 nm)	100 nm	Combined (50,100 nm)	50 nm
-4	0.09	0.11	0.22	0.30
-3	0.16	0.22	0.08	0.08
-2	0.2	0.21	0.17	0.21
-1	0.33	0.38	0.18	0.31
0	0.12	0.05	0.27	0.08
1	0.1	0.02	0.08	0.02

[a]Reported volatility distributions are fitted with $\gamma_e = 0.25$ and ΔH_{vap} = 100 KJ mol^{-1} combination

S3: Conversion equations for TD-fitted particle-phase distribution (x_i) to total (gas+particle) distribution (f_i) under a gas-particle equilibrium condition.

$$C_{tot,\mathrm{i}} = \frac{x_i C_{OA}}{\left(1+\frac{C_i^*}{C_{OA}}\right)^{-1}} \qquad \text{[Eq. S1]}$$

$$f_i = \frac{C_{tot,\mathrm{i}}}{\sum C_{tot,\mathrm{i}}} \qquad \text{[Eq. S2]}$$

Here,

$C_{tot,i}$ (μg m^{-3}): total vapor- and particle-phase mass concentration of compound *i*,

C^*_i (μg m^{-3}): effective saturation concentration of compound *i* at a reference temperature (T_{ref})

C_{OA} (μg m^{-3}): total particle-phase organic mass concentration

x_i : mass fraction of compound i found in the particle phase

f_i : fraction of the total vapor and particle-phase contributed by species *i*

Temperature dependent C_i^* is estimated from the Clausius-Clapyeron Equation (Eq. S3)

$$C_i^*(T) = C_i^*(T_{ref}) \exp\left[\frac{\Delta H_{vap,i}}{R}\left(\frac{1}{T_{ref}}-\frac{1}{T}\right)\right]\frac{T_{ref}}{T} \qquad \text{[Eq. S3]}$$

where ΔH_{vap} (kJ mol^{-1}) is the enthalpy of vaporization, R the gas constant, and T_{ref} the reference temperature (298 K).

References

Donahue, N. M., Robinson, A. L., Stanier, C. O. and Pandis, S. N.: Coupled Partitioning, Dilution, and Chemical Aging of Semivolatile Organics, Environ. Sci. Technol., 40(8), 2635–2643, doi:10.1021/es052297c, 2006.

May, A. A., Presto, A. A., Hennigan, C. J., Nguyen, N. T., Gordon, T. D. and Robinson, A. L.: Gas-particle partitioning of primary organic aerosol emissions: (1) Gasoline vehicle exhaust, Atmos. Environ., 77, 128–139, doi:10.1016/j.atmosenv.2013.04.060, 2013.

Ng, N. L., Canagaratna, M. R., Jimenez, J. L., Zhang, Q., Ulbrich, I. M. and Worsnop, D. R.: Real-Time Methods for Estimating Organic Component Mass Concentrations from Aerosol Mass Spectrometer Data, Environ. Sci. Technol., 45(3), 910–916, doi:10.1021/es102951k, 2011.

Ranjan, M., Presto, A. A., May, A. A. and Robinson, A. L.: Temperature Dependence of Gas–Particle Partitioning of Primary Organic Aerosol Emissions from a Small Diesel Engine, Aerosol Sci. Technol., 46(1), 13–21, doi:10.1080/02786826.2011.602761, 2012.

Saha, P. K., Khlystov, A. and Grieshop, A. P.: Determining Aerosol Volatility Parameters Using a “Dual Thermodenuder” System: Application to Laboratory-Generated Organic Aerosols, Aerosol Sci. Technol., 49(8), 620–632, doi:10.1080/02786826.2015.1056769, 2015.